EUROPEAN MECHANICAL SCIENCE

Research Article

e-ISSN: 2587-1110

Investigation of monolayer anodized TiO_2 film and bilayer spin coated graphene film on corrosion and tribocorrosion properties of Ti45Nb alloy

Muhammet Taha Acar[1*]

[1]Erzincan Binali Yıldırım University, Faculty of Engineering, Department of Mechanical Engineering, Erzincan, Türkiye

Orcid: M. T. Acar (0000-0002-8367-9623)

Abstract: This study investigates the structural, corrosion, and tribocorrosion properties of Ti45Nb alloy coated with monolayer and bilayer films. Ti45Nb samples were ultrasonically degreased, anodized in a H_2SO_4 and H_3PO_4 solution, and coated with graphene oxide (GO) films via spin coating and subsequent annealing. The anodized samples exhibited anatase and rutile phases, while GO films displayed characteristic Raman shifts indicating graphite oxidation. Corrosion tests in simulated body fluid (SBF) revealed enhanced corrosion resistance in bilayer samples, evidenced by a lower corrosion current density (2.28×10^{-6} A/cm^2) and a higher corrosion potential (10 mV) compared to monolayer and untreated samples. Electrochemical impedance spectroscopy (EIS) indicated superior charge transfer resistance (9.72 Ωcm^2) for bilayer coatings. Tribocorrosion tests demonstrated reduced wear rates and coefficient of friction (COF) in bilayer films, attributed to increased surface hardness and load-carrying capacity. The findings suggest that the bilayer coating significantly enhances the corrosion and tribocorrosion resistance of Ti45Nb, making it a promising material for biomedical applications.

Keywords: Graphene, Thin film, Tribology, Corrosion, TiO_2, Ti45Nb.

1. Introduction

The excellent strength qualities and low specific gravity of titanium and its alloys make them desirable materials for use in several applications [1][2]. Though they vary based on climatic conditions and regions of usage, titanium and its alloys are susceptible to wear and corrosion over time, much like other metals, which results in substantial economic losses [3]. Because of this, a great deal of research has been done on protective coatings that shield metals and alloys from wear and corrosion [4][5]. Titanium and its alloys are particularly well-suited for usage in biomedical applications because of their biocompatibility. Therefore, the development of a cost-effective and biocompatible surface coating has been the main focus of efforts in recent years to improve the resistance to wear and corrosion of titanium and its alloys [6][7].

In comparison to other titanium alloys, Ti45Nb possesses a lower Young's modulus and greater corrosion resistance, rendering it a popular choice for biomedical applications [8]. Numerous experiments have been conducted to improve the wear and corrosion resistance with the surface coating, despite the high corrosion resistance of Ti45Nb material [9]. Because it has been discovered that these qualities become insufficient when simultaneously exposed to wear, corrosion and an acidic environment [10]. In addition, due to their poor tribological performance, residues can accumulate and grow in human tissues and also dissolve in blood. Some health problems, such as inflammation and carcinogenic responses, may occur due to these consequences, and bone loss that may result from this is among the possible possibilities [11].

Oxide-based coatings are commonly utilized to improve

*Corresponding author:
Email: taha.acar@erzincan.edu.tr

Cite this article as:
Acar, M. (2024). Investigation of monolayer anodized TiO2 film and bilayer spin coated graphene film on corrosion and tribocorrosion properties of Ti45Nb alloy. *European Mechanical Science*, *8*(3): 191-198. https://doi.org/10.26701/ems.1485412

History dates:
Received: 16.05.2024, *Revision Request*: 07.06.2024, *Last Revision Received*: 09.07.2024, *Accepted*: 12.07.2024

© Author(s) 2024. This work is distributed under https://creativecommons.org/licenses/by/4.0/

the corrosion, tribocorrosion, and wear resistance of Ti45Nb material, as seen in the literature [12]. A review of the literature reveals that many experiments on oxide-based protective coatings use the TiO_2 structure. Because it is known that TiO_2, in addition to having a biocompatible structure, also increases wear resistance and corrosion resistance [13][14]. As a result, it has been noted that a variety of surface treatments, including anodic oxidation, chemical vapor deposition, physical vapor deposition, and sol-gel coating, can produce TiO_2 structure on titanium surfaces [15].

However, monolayer coatings have been replaced by bilayer coatings. Because it is known from experimental research that bilayer coatings have more benefits than monolayer coatings. It has been noted that bilayer coatings exhibit more toughness than nonolayer coatings, that increasing the hardness increases wear resistance, and that the structures in between the layers act as a protective barrier against corrosion [16][17]. Çomaklı et al. [11] created multilayer films with TiO_2-SiO_2 structures on β-type Ti45Nb alloy substrates. As a result, they highlighted that the values of multilayer film-coated substrates were higher than those of untreated substrates in terms of wear resistance, corrosion resistance, and surface hardness. Wei et al. [18] investigated the surface hardness of multilayer structures and found that for samples with multilayer coatings, the maximum hardness was reached approximately 3 times greater than that of the substrate material.

As a result of the analysis of the studies, it was observed that the wear and corrosion resistance of titanium alloys increased with double-layer structures. In order to further increase the wear and corrosion resistance, it is thought that the use of graphene-based structures together with the TiO_2 structure will increase the corrosion and wear resistance of titanium materials to the desired level. In previous studies using graphene-based structures, it was stated that wear and corrosion resistance increased. Chen et al. [19] emphasized that graphene nanolayers well dispersed improved the anti-corrosion performance and wear resistance properties.

In this research, graphene is coated on TiO_2 using a spin coating process, and TiO_2 anodic layer is formed on Ti45Nb by anodization method, which is commonly employed mainly in biomedical applications since it encourages bone formation on titanium surfaces. Examining the corrosion and tribocorrosion characteristics of monolayer TiO_2 and bilayer TiO_2-graphene coatings on Ti45Nb is the aim of this study. The structural characterization of the samples was performed using X-ray diffraction (XRD), Raman spectroscopy, and scanning electron microscopy (SEM) techniques. By using potentiodynamic polarization and open circuit potential (OCP) approaches, electrochemical characteristics were examined and their tribocorrosion characteristics in simulated body fluid (SBF) were investigated and contrasted.

2. Methodology

2.1. Sample preparation

In this study, Ti45Nb samples with their chemical composition as provided in ▶Table 1 were utilized [20]. Ti45Nb samples with dimensions of 1.5*1.5 cm^2 and 3 mm in thickness were ultrasonically degreased in acetone and ethanol for 20 minutes, respectively, then dried after being cleaned one more with an ultrasonic cleaner and distilled water.

Table 1. The chemical composition of Ti45Nb (wt%).

Substrate	Ti	Nb (max)	Others
Ti45Nb	54.69	45.11	0.2

2.2. Experimentation

The electrolytes were utilized to make the anodization solution H_2SO_4 = 0.75 molar and H_3PO_4 = 0.5 molar as described in our previous study [21][22]. Before anodization, the Ti45Nb sample was immersed in HNO_3 for a minute. It was then rinsed with distilled water and dried. A graphite rod served as the negative electrode and a Ti45Nb sample as the positive electrode. During

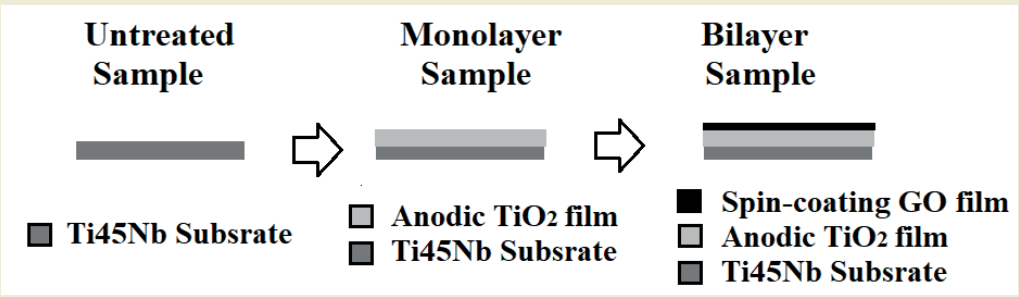

Figure 1. Schematic diagram of the coating processes of the monolayer TiO_2 and bilayer TiO_2-GO films on Ti45Nb samples with anodization and spin-coating methods.

the anodization process, the distance between them was fixed at 30 mm. The anodic layer was formed in the prepared solution by applying a voltage of 200 V to the samples and letting them anodize for 20 minutes at room temperature. After that, the sample was dried and rinsed with distilled water. As shown Fig.1 to make the graphene oxide films (GO), the graphite oxide flakes were dissolved in deionized water at a concentration of 10 mg/ml. The solution was sonicated for thirty minutes, and then it was swirled for two hours. The solution was then spin-coated onto the substrate for 30 seconds at 3500 rpm to form GO film. GO films were then annealed for 30 minutes at 500°C in an argon atmosphere to produce conductive graphene films [23]. All coatings were repeated 3 times to check their reproducibility.

Using a Cu-K (=1.54059) source operated at 40 kV and 30 mA, an XRD-GNR-Explorer X-Ray diffraction apparatus was used to determine the phase of Ti45Nb samples on a 2θ scale spanning from 10° to 80°. By comparing them to the International Diffraction Data Center (ICDD) standard cards, all phases were identified. Using a WITec alpha 300 R instrument with a 532 nm wavelength and 0.3 mWatt of power, the Raman studies were conducted. Using the FEI QUANTA 250 Scanning Electron Microscope, pictures of the top and cross-section were captured. Vickers microhardness measurements were performed using a Buehler Micromet device with an average obtained from five distinct spots and a loading duration of 10 s under a 10 g load.

All experimental parameters used in corrosion and tribocorrosion experiments and the chemical composition of the SBF liquid in which the experiments were carried out are given in our previous study [22].

The GAMRY series G750TM (Gamry Instruments, Warminster, USA) with potentiodynamic polarization was used for the electrochemical investigations. Using a heater, the SBF temperature was set and maintained during the tribocorrosion and corrosion tests. The samples of Ti45Nb underwent corrosion resistance testing at 37 ± 0.5 °C. The three-electrode method was applied in the electrochemical experiments [24]. The reference electrode was Ag/AgCl, and the counter electrode was graphite. The prior study provided the basic test parameters for electrochemical analyses.

At 50% relative humidity, tribocorrosion tests were conducted using the Turkyus PODWT&RWT reciprocating tribotester and electrochemical monitoring apparatus. After potential equilibration, tribocorrosion rubbing experiments were carried out in open-circuit potential settings. The pin was an Al_2O_3 ball with a 6 mm diameter, and 1 N of normal force was applied as for ASTM G133-02. The stroke had a length of 8 mm and a frequency of 1 Hz of reciprocation. A Bruker Contour GT-K1 3D surface profilometer was used to investigate the wear depth. In order to verify the test results, all corrosion and tribocorrosion experiments were repeated 3 times.

3. Results and discussion

3.1. Structural characterization

Fig. 2-a illustrates the XRD patterns for the untreated, monolayer, and bilayer samples. The XRD patterns revealed the presence of β-Ti peaks in the Ti45Nb substrate. It was observed that the monolayer TiO_2 film formed on the substrate during the anodization process consisted of both anatase and rutile phases. Previous investigations, based on XRD data, demonstrated the compatibility of rutile and anatase structures [21]. The presence of GO structures in the XRD spectrum of the bilayer film was confirmed by a broad peak in the range of approximately 24°-25° on Ti45Nb [25].

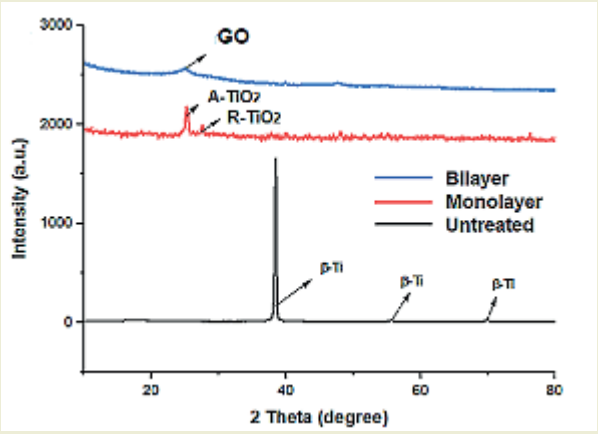

(a)

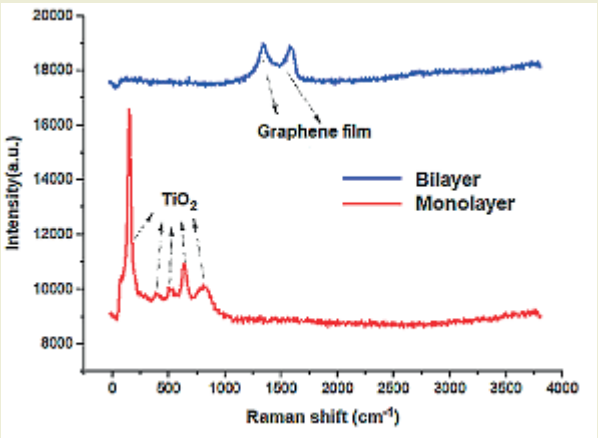

(b)

Figyre 2. **(a)** XRD graphs, **(b)** Raman spectra of untreated, monolayer, and bilayer Ti45Nb samples

▶**Figure 2-b** displays the Raman spectra of the monolayer and bilayer samples. It can be demonstrated that Raman spectra of the anatase crystal phase exhibit five distinct bands. The maximums were approximately

144, 196, 391, 514, and 634 cm^{-1}, and they matched the active modes Eg(1), Eg(2), B1g, A1g, and Eg(3) respectively. Because the Raman spectra only show the bulk material and not the pores in the structures formed in the anodic films, where the rutile phase is concentrated near the open pores, they only show the anatase phase. All anodized Ti45Nb samples have the anatase phase as the primary phase, according to Raman spectra. ▶**Figure 2**-b GO Raman spectra show the shift in GO structure brought on by graphite oxidation, with the G (sp^2) band corresponding to structures. Conversely, oxidation results in uneven, amorphous structures in the D (sp^3) band. The GO G-band and D-band are visible at 1595 $cm^{-1}$and 1360 cm^{-1}, respectively. In graphite, the G-band is present in all sp2 carbon systems due to the stretching of the C-C bond. Structural flaws resulting from epoxy and hydroxyl group attachment to the GO basal plane give rise to the D-band [26].

Figure 3 presents cross-sectional view images of the bilayer sample and top-view SEM images of the untreated, monolayer, and bilayer samples. The sample exhibits small open pores on its surface following anodization. The formation of micropores is consistent with prior

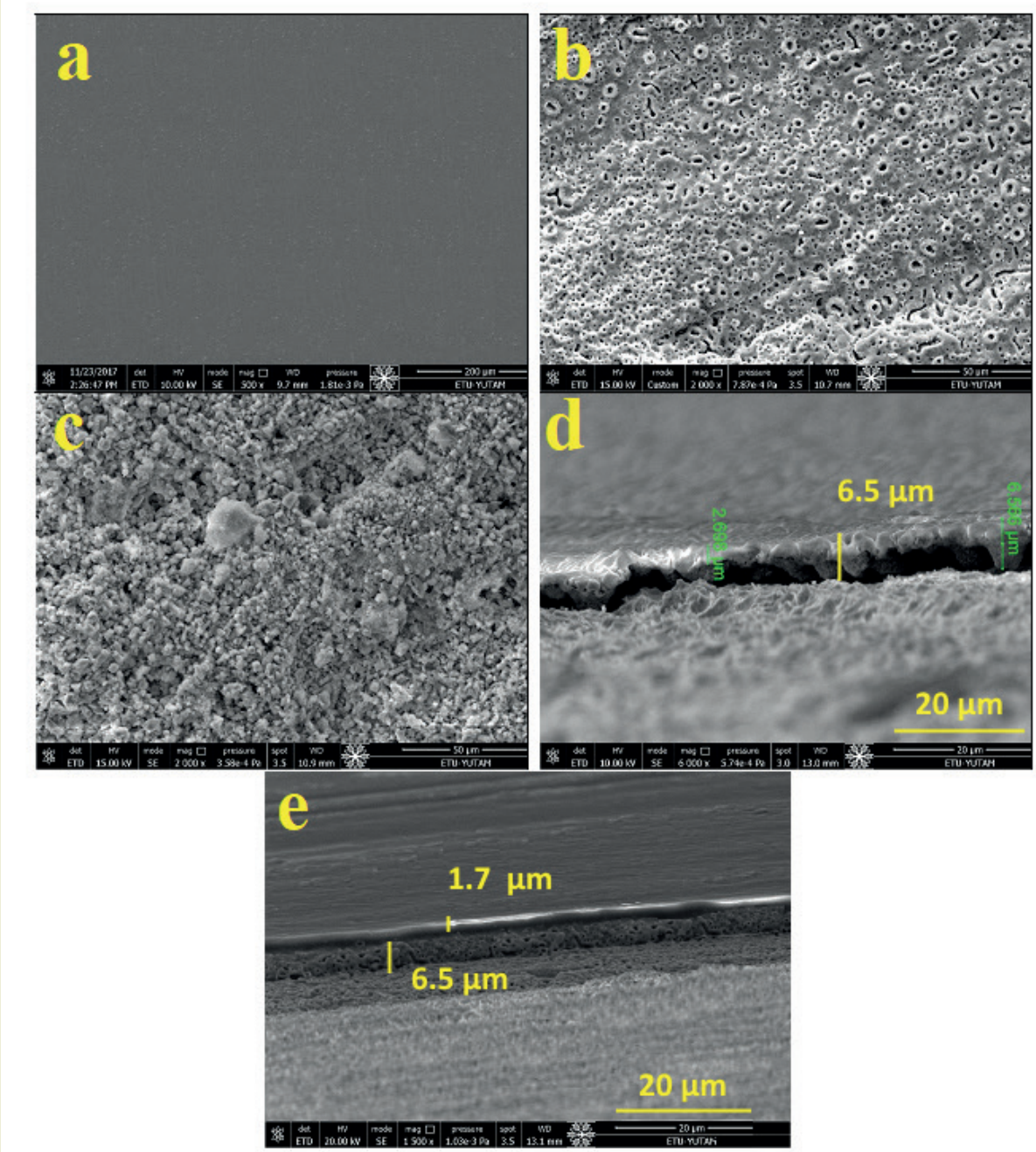

Figure 3. SEM images of **(a)** untreated, **(b)** monolayer, and **(c)** bilayer Ti45Nb samples **(d)** cross-section SEM image of monolayer sample and **(e)** cross-section SEM image of bilayer sample

studies [21]. It is evident from the SEM image that there are additional nanopores formed due to the presence of oxygen. Nanopores are generated during the anodizing process when oxygen bubbles form as a result of the oxidation reaction [27]. The SEM image of the graphene structure fabricated on TiO_2 using the spin coating technique reveals a change in surface morphology. It is hypothesized that the action of centrifugal force induces dense clustering of graphene structures around open pores. Analysis of the cross-section SEM image indicated a thickness of 1.7 µm for the graphene film, while the TiO_2 anodic layer measured 6.5 µm.

3.2. Corrosion experiment

The potentiodynamic polarization curves for untreated, monolayer, and bilayer materials in SBF solution are depicted in ▶**Figure 4-a**. These curves were obtained through electrochemical testing. ▶**Table 2** presents the

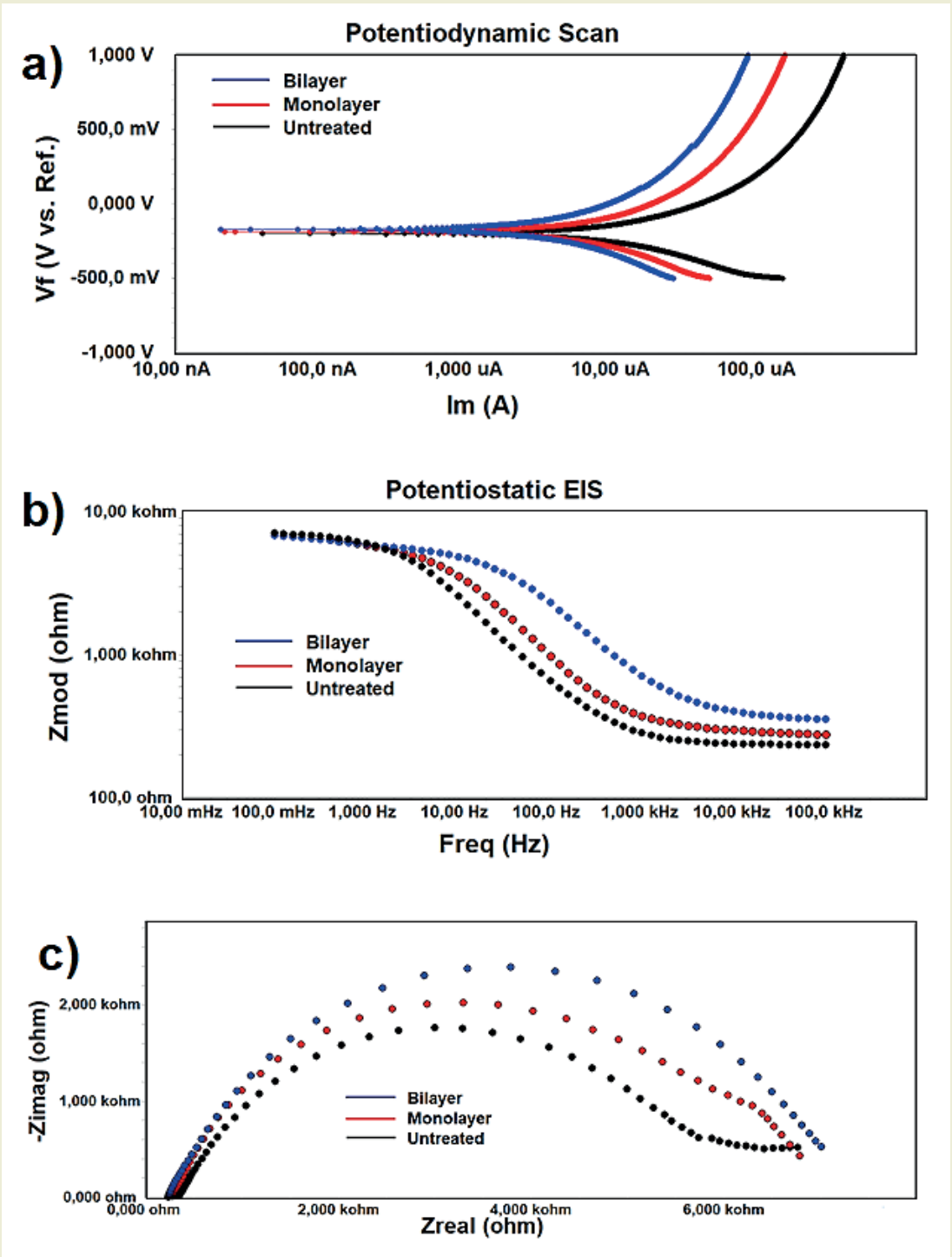

Figure 4. (a) Potentiodynamic polarization curves, **(b)** Bode, and **(c)** Nyquist plots of untreated, monolayer, and bilayer Ti45Nb samples

corrosion potential (Ecorr) and corrosion current density (Icorr) values derived from the polarization curves. Lower Icorr values and higher Ecorr values indicate greater corrosion resistance [28]. When compared to untreated samples, both monolayer and bilayer samples demonstrate higher corrosion current density and lower corrosion potential. In contrast, the bilayer sample exhibits lower corrosion Icorr ($2.28x10^{-6}$ A/cm^2) and greater positive Ecorr (10 mV) values than the monolayer sample. The bilayer sample exhibits the best corrosion resistance due to its greater film thickness, which creates an interface acting as a barrier, thereby preventing contact between the SBF liquid and the Ti45Nb substrate [29].

The Bode and Nyquist plots are presented in ▶**Figure 4-b** and ▶**Figure 4-c**, respectively. The results of the simulated EIS are shown in ▶**Table 2**. The charge transfer resistance (Rct) is a critical parameter for assessing a electrochemistry of samples. It represents the rate of corrosion between the coating and the substrate [30]. Due to the thinner oxide layer on untreated Ti45Nb compared to anodized samples, the Rct is lower. Additionally, the presence of anatase and rutile oxide enhances the performance of anodized samples as insulators with lower capacitance. When the corrosion resistance of the bilayer film (9.72 Ωcm^2) is compared with the corrosion resistance of the monolayer film (6.56 Ωcm^2), it has been discovered that the corrosion resistance of the bilayer film is higher. It has been established that in this case, the interlayer spacing and film thickness play significant roles in corrosion resistance [31]. As a result, the bilayer coating displayed maximum corrosion resistance, making it more challenging for SBF to reach the substrate.

3.3. Tribocorrosion experiment

The open circuit potential (OCP) graphs of the untreated, monolayer, and bilayer Ti45Nb samples are depicted in Fig. 5-a. Initially, during the rubbing process, the OCP curve of the untreated sample exhibited the largest reduction compared to the other samples once the system reached equilibrium. This reduction in OCP values (-650mV) for the untreated Ti45Nb sample was attributed to damage caused to the natural oxide film by the surface treatment. OCP values of -150 mV and -40 mV were observed for the monolayer and bilayer samples, respectively. It was observed that after the onset of the friction process, the OCP values of the monolayer sample decreased at a slower rate compared to those of the untreated sample. As expected, the rubbing action on the bilayer film resulted in the highest average OCP values.

The average COF for the untreated sample ranged between 0.35 and 0.45. Average COF values ranging from 0.26 to 0.36 were obtained in the monolayer film. Additionally, the lowest average COF values were obtained from the bilayer film, ranging from 0.17 to 0.22. The higher COF values observed in the untreated sample are associated with the breakdown of the oxide layer on pure titanium alloys due to wear and corrosion, resulting in residues that cause abrasive wear [32].

As seen in ▶**Figure 5-b** and ▶**Figure 5-c** the untreated sample has the highest wear rate ($0.72\ x10^{-3}$ mm^3/Nm), whereas the bilayer sample has the lowest wear rate ($0.12\ x10^{-3}$ mm^3/Nm). In addition to the formation of an interface between the bilayer films serving as a protective barrier against corrosion, their higher load-carrying capacity has increased the tribocorrosion resistance of the bilayer film. The presence of the interface was found to enhance the load-carrying capacity of bilayer coatings compared to monolayer films in previous studies [11]. The bilayer surfaces prevent dislocation and reduce the system's plastic deformation, thereby increasing its hardness. According to Archard's rule, higher surface hardness reduces the contact between the wear ball and the films, resulting in the minimum wear rate being achieved in the bilayer film with maximum hardness [33].

Consequently, the influence of increasing layer thickness and obtained surface hardness on corrosion and tribocorrosion resistance is evident when Fig. 3-c and ▶**Table 2** are compared. However, the advantages gained in the bilayer film have a greater impact here. According to the literature, the interlayer in the bilayer coating enhanced resistance to corrosion and tribocorrosion by lowering internal tensions, allowing displacement movement, and exhibiting a barrier effect against corrosion [34].

4. Conclusions

In this study, the corrosion and tribocorrosion resistance of Ti45Nb samples coated with graphene oxide (GO) films were systematically investigated.

Table 2. Results of tests performed on all samples for film thickness, hardness, corrosion, and tribocorrosion.

	E_{corr} (mV)	i_{corr} (x10–^{6}A/cm^2)	Rct (Ωcm^2)	Film thickness (μm)	Hardness ($HV_{0.1}$)	COF	Wear rate (x10^{-3} mm^3/Nm)
Bilayer	10	2.28	9.72	6.5+1.7	1270	0.17-0.22	0.14
Monolayer	-163	40.24	6.56	6.5	765	0.26-0.36	0.58
Untreated	-285	72.86	3.84	-	378	0.35-0.45	0.72

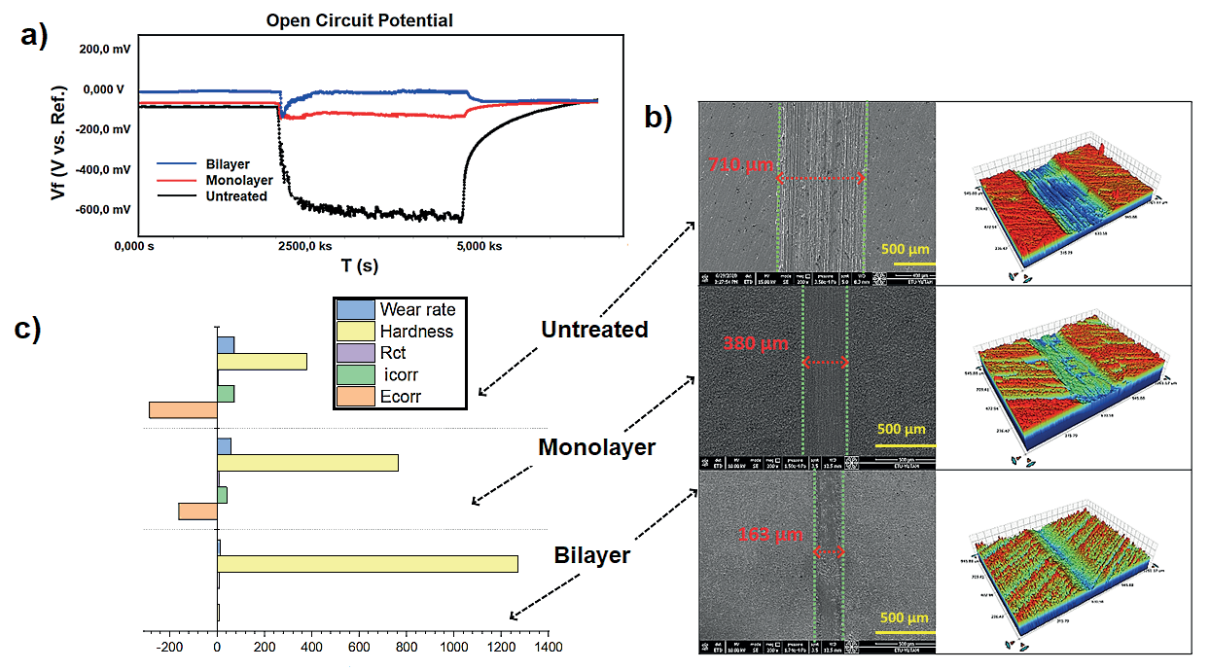

Figure 5. **(a)** Open circuit potential, **(b)** 3D profilometer and SEM images **(c)** graphical presentation of the all data of untreated, monolayer, and bilayer Ti45Nb samples

- The results demonstrated that the bilayer GO films exhibited superior corrosion resistance compared to monolayer films and untreated samples. This enhanced performance is attributed to the increased film thickness and the presence of an interfacial layer, which acts as an effective barrier against simulated body fluid (SBF) penetration.

- The XRD and Raman spectroscopy analyses confirmed the formation of anatase and rutile phases in the anodized TiO_2 layer and the successful incorporation of GO structures in the bilayer films.

- The electrochemical tests revealed that the bilayer samples exhibited the lowest corrosion current density (Icorr) and the most positive corrosion potential (Ecorr), indicating their excellent corrosion resistance.

- The tribocorrosion experiments further validated these findings, with the bilayer samples showing the highest open circuit potential (OCP) and the lowest coefficient of friction (COF) and wear rate. The significant reduction in wear rate and improved tribocorrosion resistance are due to the enhanced load-carrying capacity and hardness provided by the bilayer films.

These results contribute to the growing body of knowledge on the use of graphene-based coatings in enhancing the performance of biomedical implants, paving the way for further innovations in the field of biomaterials engineering.

Research Ethics

Ethical approval not required.

Author Contributions

All authors contributed to the study conception and design. Material preparation, data collection and analysis were performed by [M. Taha ACAR].

Conflicts of interests

The authors declare that they have no known competing financial interests or personal relationships that could have appeared to influence the work reported in this paper.

Research Funding

Not reported.

Data availability

Data supporting this study are included within the article.

Peer-review

Externally peer-reviewed.

References

[1] Boyer, R. R. (1996). An overview on the use of titanium in the aerospace industry. *Materials Science and Engineering: A, 213*, 103–114.

[2] Acar, M. T. (2023). Investigation of surface wettability, corrosion and tribocorrosion behavior of machined, etched, blasted and anodized Cp-Ti samples. *MRS Communications, 13*, 587–593. https://doi.org/10.1557/s43579-023-00387-6

[3] Geetha, M., Singh, A. K., Asokamani, R., & Gogia, A. K. (2009). Ti based biomaterials, the ultimate choice for orthopaedic implants–a review. *Progress in Materials Science, 54*, 397–425.

[4] Hoque, M. A., Yao, C.-W., Lian, I., Zhou, J., Jao, M., & Huang, Y.-C. (2022). Enhancement of corrosion resistance of a hot-dip galvanized steel by superhydrophobic top coating. *MRS Communications, 12*, 415–421.

[5] Guo, C., Kang, T., Wu, S., Ying, M., Liu, W. M., & Chen, F. (2021). Microstructure, mechanical, and corrosion resistance of copper nickel alloy fabricated by wire-arc additive manufacturing. *MRS Communications, 11*, 910–916.

[6] Bandyopadhyay, A., Bose, S., & Narayan, R. (2022). Translation of 3D printed materials for medical applications. *MRS Bulletin, 47*, 39–48.

[7] Rathnakumar, S., Bhaskar, S., Badiya, P. K., Sivaramakrishnan, V., Srinivasan, V., & Ramamurthy, S. S. (2023). Electrospun PVA nanofibers doped with titania nanoparticles in plasmon-coupled fluorescence studies: An eco-friendly and cost-effective transition from 2D nano thin films to 1D nanofibers. *MRS Communications, 13*, 290–298.

[8] Comakli, O. (2020). Influence of CrN, TiAlN monolayers and TiAlN/CrN multilayer ceramic films on structural, mechanical and tribological behavior of β-type Ti45Nb alloys. *Ceramics International, 46*, 8185–8191.

[9] Çomaklı, O. (2021). Improved structural, mechanical, corrosion and tribocorrosion properties of Ti45Nb alloys by TiN, TiAlN monolayers, and TiAlN/TiN multilayer ceramic films. *Ceramics International, 47*, 4149–4156.

[10] Laketić, S., Rakin, M., Momčilović, M., Ciganović, J., Veljović, D., & Cvijović-Alagić, I. (2021). Influence of laser irradiation parameters on the ultrafine-grained Ti45Nb alloy surface characteristics. *Surface and Coatings Technology, 418*, 127255.

[11] Çomaklı, O., Yazıcı, M., Demir, M., Yetim, A. F., & Çelik, A. (2023). Effect of bilayer numbers on structural, mechanical, tribological and corrosion properties of TiO2–SiO2 multilayer film-coated β-type Ti45Nb alloys. *Ceramics International, 49*, 3007–3015.

[12] Zorn, G., Lesman, A., & Gotman, I. (2006). Oxide formation on low modulus Ti45Nb alloy by anodic versus thermal oxidation. *Surface and Coatings Technology, 201*, 612–618.

[13] Yin, J., Chu, Y., & Tan, L. (2023). Cu/N co-doped TiO2 nanopowder with high antibacterial activity under visible light. *MRS Communications*. https://doi.org/10.1557/s43579-023-00377-8

[14] Krishna, D. S. R., & Sun, Y. (2005). Thermally oxidised rutile-TiO2 coating on stainless steel for tribological properties and corrosion resistance enhancement. *Applied Surface Science, 252*, 1107–1116.

[15] Kulkarni, M., Mazare, A., Schmuki, P., Iglič, A., & Seifalian, A. (2014). Biomaterial surface modification of titanium and titanium alloys for medical applications. *Nanomedicine, 111*, 111.

[16] PalDey, S., & Deevi, S. C. (2003). Single layer and multilayer wear resistant coatings of (Ti, Al) N: A review. *Materials Science and Engineering: A, 342*, 58–79.

[17] Ding, Z., Zhou, Q., Wang, Y., Ding, Z., Tang, Y., & He, Q. (2021). Microstructure and properties of monolayer, bilayer and multilayer Ta-2O5-based coatings on biomedical Ti-6Al-4V alloy by magnetron sputtering. *Ceramics International, 47*, 1133–1144.

[18] Wei, Y., & Gong, C. (2011). Effects of pulsed bias duty ratio on microstructure and mechanical properties of TiN/TiAlN multilayer coatings. *Applied Surface Science, 257*, 7881–7886.

[19] Chen, W., Yang, Y., Zhao, Q., Liu, X., & Fu, Y.-Q. (2022). Nanoscale mechanics of metal-coated graphene nanocomposite powders. *Materials Today Communications, 33*, 104731.

[20] Acar, M. T., Kovacı, H., & Çelik, A. (2022). Comparison of the structural properties, surface wettability and corrosion resistance of TiO2 nanotubes fabricated on Cp-Ti, Ti6Al4V and Ti45Nb. *Materials Today Communications, 33*, 104396.

[21] Acar, M. T., Kovacı, H., & Çelik, A. (2022). Improving the wettability and corrosion behavior of Cp-Ti by applying anodization surface treatment with the addition of boric acid, graphene oxide and hydroxyapatite. *Materials Today Communications, 31*, 103683. https://doi.org/10.1016/j.mtcomm.2022.103683

[22] Acar, M. T. (2024). Analyzing the corrosion and tribocorrosion performances of monolayer TiO2 and bilayer TiO2-SiO2 coatings at different SBF temperatures. *Physica Scripta, 99*, 025910.

[23] Umar, M. I. A., Yap, C. C., Awang, R., Salleh, M. M., & Yahaya, M. (2014). The effect of spin-coated polyethylene glycol on the electrical and optical properties of graphene film. *Applied Surface Science, 313*, 883–887.

[24] Salasi, M., Stachowiak, G. B., & Stachowiak, G. W. (2011). Three-body tribocorrosion of high-chromium cast irons in neutral and alkaline environments. *Wear, 271*, 1385–1396. https://doi.org/10.1016/j.wear.2011.01.066

[25] Wang, Y., Wang, S., Wu, Y., Wang, Z., Zhang, H., Cao, Z., He, J., Li, W., Yang, Z., & Zheng, L. (2021). A α-Fe2O3/rGO magnetic photocatalyst: Enhanced photocatalytic performance regulated by magnetic field. *Journal of Alloys and Compounds, 851*, 156733.

[26] Oktay, A., Yilmazer, H., Przekora, A., Yilmazer, Y., Wojcik, M., Dikici, B., & Ustundag, C. B. (2023). Corrosion response and biocompatibility of graphene oxide (GO) serotonin (Ser) coatings on Ti6Al7Nb and Ti29Nb13Ta4.6Zr (TNTZ) alloys fabricated by electrophoretic deposition (EPD). *Materials Today Communications, 34*, 105236.

[27] Li, X., Li, C., Gong, T., Su, J., Zhang, W., Song, Y., & Zhu, X. (2021). Comparative study on the anodizing process of Ti and Zr and oxide morphology. *Ceramics International, 47*, 23332–23337.

[28] Mansfeld, F., Liu, G., Xiao, H., Tsai, C. H., & Little, B. J. (1994). The corrosion behavior of copper alloys, stainless steels and titanium in seawater. *Corrosion Science, 36*, 2063–2095.

[29] Marcus, P., Maurice, V., & Strehblow, H.-H. (2008). Localized corrosion (pitting): A model of passivity breakdown including the role of the oxide layer nanostructure. *Corrosion Science, 50*, 2698–2704.

[30] Dehri, I., & Erbil, M. (2000). The effect of relative humidity on the atmospheric corrosion of defective organic coating materials: An EIS study with a new approach. *Corrosion Science, 42*, 969–978.

[31] Volovitch, P., Vu, T. N., Allély, C., Aal, A. A., & Ogle, K. (2011). Understanding corrosion via corrosion product characterization: II. Role of alloying elements in improving the corrosion resistance of Zn-Al-Mg coatings on steel. *Corrosion Science, 53*, 2437–2445.

[32] Khan, M. A., Williams, R. L., & Williams, D. F. (1999). Conjoint corrosion and wear in titanium alloys. *Biomaterials, 20*, 765–772.

[33] Acar, M. T., Kovacı, H., & Çelik, A. (2022). Investigation of corrosion and tribocorrosion behavior of boron doped and graphene oxide doped TiO2 nanotubes produced on Cp-Ti. *Materials Today Communications, 32*, 104182.

[34] Çomaklı, O. (2021). Improved structural, mechanical, corrosion and tribocorrosion properties of Ti45Nb alloys by TiN, TiAlN monolayers, and TiAlN/TiN multilayer ceramic films. *Ceramics International, 47*, 4149–4156.